

DAMPING RESONANT CURRENT IN A SPARK-GAP TRIGGER CIRCUIT TO REDUCE NOISE

E. L. Ruden

*Air Force Research Laboratory, Directed Energy Directorate,
AFRL/RDHP, 3550 Aberdeen Blvd. SE, Kirtland AFB, NM 87117-5776 USA*

D. J. Brown, M. R. Kostora, T. C. Grabowski, C. W. Gregg, B. M. Martinez, J. V. Parker

Science Applications International Corporation, 2109 Air Park Rd SE, Albuquerque, NM 87106 USA

J. F. Camacho, S. K. Coffey

NumerEx, 2309 Renard Place SE, Albuquerque, NM 87016 USA

P. Poulsen

CARE'N Co. Livermore, CA 94551 USA

Abstract

Radio frequency (RF) interference (noise) caused by the triggering of spark-gap switched pulsed-power circuits is a significant problem for electronic diagnostics. Traditional approaches to mitigation involve using RF-tight enclosures, noise resistant diagnostic designs, power filtering, and/or time-integration of signals. These approaches can be costly, and not always successful. A detailed study of the source of this noise is undertaken motivated by an experiment using a charged coaxial cable triggered rail-gap (multichannel linear spark-gap) switched system based on a quarter-module of AFRL's Shiva Star Capacitor Bank. For this, the noise interferes with an unintegrated measurement needed of the load's local electric field. The noise source is identified as resonant current oscillation after rail-gap closure in the circuit triggering the rail-gaps. The solution in this case is to replace the $50\ \Omega$ trigger cable with one with half that impedance, and install a carbon composite resistor in series with the cable output with a resistance equal to the new cable's impedance. The output impedance of the trigger circuit and, therefore, the rail-gap current behavior during breakdown is thereby preserved, but reflections back into the cable after switch closure are minimized by impedance matched resistance termination. In practice, termination is compromised by lead inductance and blocking capacitors, but near-critical damping of subsequent resonant behavior is nonetheless observed. A circuit model of this behavior is validated to help adapt and optimize the technique for other systems.

I. INTRODUCTION

Experiments are performed on a $36\ \mu\text{F}$ capacitor bank (Fig. 1) charged to 21 kV and discharged through two parallel rail-gaps (Maxwell Model 40200)[1][2] (Fig. 2) triggered by separate charged cables connected to a single Multiple Trigger Generator (MTG)[3]. The current waveform of the main discharge is that of a weakly damped

RLC circuit with 1/4-cycle rise-time of $2.5\ \mu\text{s}$ and a peak current of 0.410 MA. Radio frequency (RF) current associated with the cable trigger circuit induces current in electronic probes measuring local electric and magnetic fields in a tamped fuse load being studied, so an effort is made to reduce such "noise" at the source. Similar capacitor and cable triggered spark and rail-gap circuits are commonly used in other pulsed power systems, and trigger noise is a common issue, so the results should be of general interest.

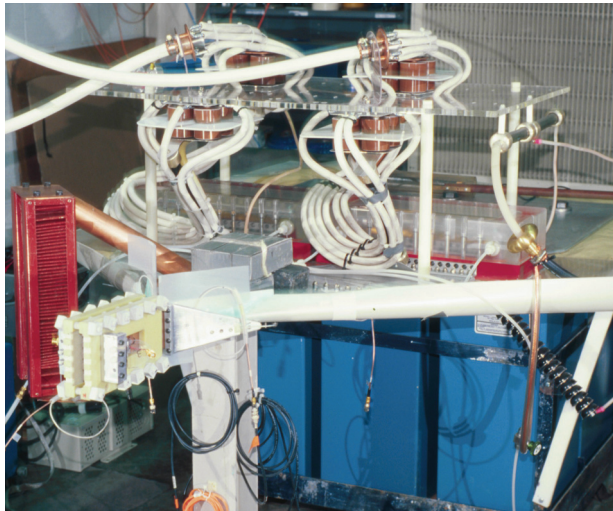


Figure 1. Capacitor bank used to test damped trigger circuit.

II. TRIGGER CIRCUIT TERMINATION/DAMPING

A simplified schematic of the charged cable rail-gap trigger circuit is shown in Fig. 3. The usual design for such a circuit does not include resistor R_2 as an explicit component (only a small incidental conductor resistance is present). It is included here for the purpose of damping

Report Documentation Page

Form Approved
OMB No. 0704-0188

Public reporting burden for the collection of information is estimated to average 1 hour per response, including the time for reviewing instructions, searching existing data sources, gathering and maintaining the data needed, and completing and reviewing the collection of information. Send comments regarding this burden estimate or any other aspect of this collection of information, including suggestions for reducing this burden, to Washington Headquarters Services, Directorate for Information Operations and Reports, 1215 Jefferson Davis Highway, Suite 1204, Arlington VA 22202-4302. Respondents should be aware that notwithstanding any other provision of law, no person shall be subject to a penalty for failing to comply with a collection of information if it does not display a currently valid OMB control number.

1. REPORT DATE

JUN 2009

2. REPORT TYPE

N/A

3. DATES COVERED

-

4. TITLE AND SUBTITLE

Damping Resonant Current In A Spark-Gap Trigger Circuit To Reduce Noise

5a. CONTRACT NUMBER

5b. GRANT NUMBER

5c. PROGRAM ELEMENT NUMBER

6. AUTHOR(S)

5d. PROJECT NUMBER

5e. TASK NUMBER

5f. WORK UNIT NUMBER

7. PERFORMING ORGANIZATION NAME(S) AND ADDRESS(ES)

Science Applications International Corporation, 2109 Air Park Rd SE, Albuquerque, NM 87106 USA

8. PERFORMING ORGANIZATION REPORT NUMBER

9. SPONSORING/MONITORING AGENCY NAME(S) AND ADDRESS(ES)

10. SPONSOR/MONITOR'S ACRONYM(S)

11. SPONSOR/MONITOR'S REPORT NUMBER(S)

12. DISTRIBUTION/AVAILABILITY STATEMENT

Approved for public release, distribution unlimited

13. SUPPLEMENTARY NOTES

See also ADM002371. 2013 IEEE Pulsed Power Conference, Digest of Technical Papers 1976-2013, and Abstracts of the 2013 IEEE International Conference on Plasma Science. IEEE International Pulsed Power Conference (19th). Held in San Francisco, CA on 16-21 June 2013., The original document contains color images.

14. ABSTRACT

Radio frequency (RF) interference (noise) caused by the triggering of spark-gap switched pulsed-power circuits is a significant problem for electronic diagnostics. Traditional approaches to mitigation involve using RF-tight enclosures, noise resistant diagnostic designs, power filtering, and/or time-integration of signals. These approaches can be costly, and not always successful. A detailed study of the source of this noise is undertaken motivated by an experiment using a charged coaxial cable triggered rail-gap (multichannel linear spark-gap) switched system based on a quarter-module of AFRLs Shiva Star Capacitor Bank. For this, the noise interferes with an unintegrated measurement needed of the loads local electric field. The noise source is identified as resonant current oscillation after rail-gap closure in the circuit triggering the rail-gaps. The solution in this case is to replace the 50 Ω trigger cable with one with half that impedance, and install a carbon composite resistor in series with the cable output with a resistance equal to the new cables impedance. The output impedance of the trigger circuit and, therefore, the rail-gap current behavior during breakdown is thereby preserved, but reflections back into the cable after switch closure are minimized by impedance matched resistance termination. In practice, termination is compromised by lead inductance and blocking capacitors, but near-critical damping of subsequent resonant behavior is nonetheless observed. A circuit model of this behavior is validated to help adapt and optimize the technique for other systems.

15. SUBJECT TERMS

16. SECURITY CLASSIFICATION OF:			17. LIMITATION OF ABSTRACT SAR	18. NUMBER OF PAGES 6	19a. NAME OF RESPONSIBLE PERSON
a. REPORT unclassified	b. ABSTRACT unclassified	c. THIS PAGE unclassified			

Standard Form 298 (Rev. 8-98)
Prescribed by ANSI Std Z39-18

cable circuit resonances. The schematic location of the charged cable with transient time τ_0 is identified by the sketched cylinder.

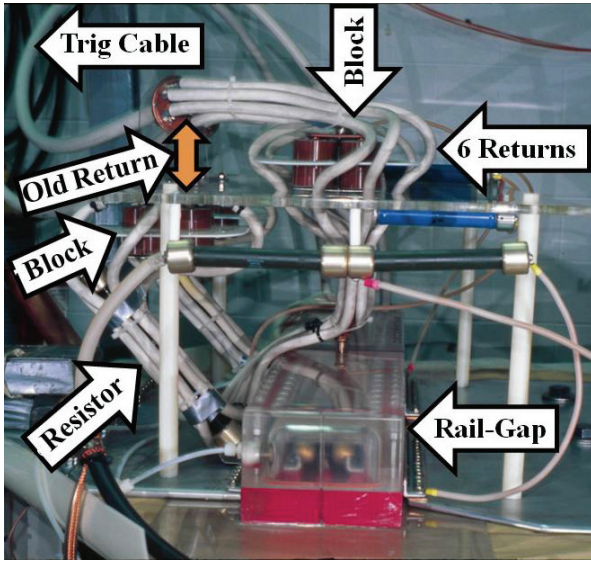


Figure 2. Rail-gap pair viewed end-on with associated trigger circuit break-out. The return conductor for the current feed from each trigger cable is carried by six parallel silicone rubber insulated high voltage wires closely enveloping the blocking capacitors and damping resistor to minimize inductance. The $28\ \Omega$ resistor of the foreground rail-gap is seen surrounded by these wires (lower left). The original cable break-out circuit formed a loop, with the ground-side blocking capacitors (middle left) connected to the cable ground via a Cu shunt plate at the location indicated by the superimposed double arrow (upper left).

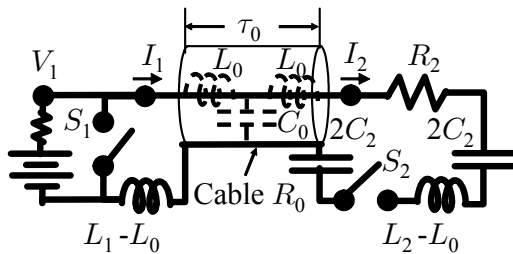


Figure 3. Simplified schematic of charged cable rail-gap trigger circuit. The low frequency response of the charged (3 m) trigger cable with impedance R_0 and transit time τ_0 may be approximated by the two-loop lumped circuit shown. The rail-gap is S_2 and the spark-gap discharging the cable, thereby triggering S_2 after delay τ_0 , is S_1 .

Each of the two rail-gaps (represented by S_2) is triggered to close after the spark-gap (S_1) in the MTG closes, shorts the end of the cable (which has been charged beforehand to voltage V_0), and launches a transverse electromagnetic (TEM) wave toward the rail-gap end.

The wave reflects off the initially open circuit, causing a voltage doubling that breaks down the gas in the rail-gap. Blocking capacitors ($2C_2$) are used to isolate the MTG from the much higher energy main capacitor bank discharge as safety measure. Subsequent multiple TEM reflections couple to circuits on both ends. The resultant normal modes of oscillation are the source of the troublesome noise.

To address the noise issue, the original $50\ \Omega$ impedance rail-gap trigger cable is replaced with a $22.5\ \Omega$ RG-17/14 insulated cable in series with a $R_0 = 28\ \Omega$ carbon composite resistor. RG-17/14 is a special order polyethylene ($\epsilon = 2.26$) insulated cable where the outer conductor of an RG-14 cable replaces the inner conductor of an RG-17 cable so as to give it a lower impedance. In this way, the output impedance of the cable plus resistor remains similar to that of the older (proven) design so as to guarantee that the current time history of the rail-gap plasma will be similar during gas break-down. That is, nominally identical rail-gap plasma behavior is preserved. However, the blocking capacitors are quadrupled relative to the original design so as to be, when placed in series, significantly larger than the cable capacitance and, therefore, behave more like a short-circuit on a cable transient time scale. Also, L_2 is substantially minimized by use of multiple current paths closely enveloping the circuit components. The ideal result, then, is that the impedance of the rail-gap end of the trigger circuit is dominated by R_2 after S_2 closure, terminating the transient. There should, therefore, be a minimal reflection of the TEM trigger wave and subsequent re-reflections from the MTG end.

As with any closed transmission line, there are an infinite number of normal modes of current oscillation possible. It is found for our experiment, however, that only the two lowest frequency modes persist for more than 200 ns. Since these modes have a much longer period than than a cable transit time, they may be represented by a two-loop circuit where the cable capacitance is lumped into C_0 of Fig. 3, the cable inductance is split evenly between inductors L_0 on either side ($L_0 = C_0 R_0^2 / 2$), and R_2 is interpreted as a harmonic damping element. The rail-gap feed is the right loop, and the MTG used to discharge the cable is on the left. Nominal circuit parameters are,

$$\begin{aligned} \tau_0 &= 18.4\ \text{ns} & C_0 &= 0.82\ \text{nF} & L_2 &= 889\ \text{nH} \\ R_0 &= 22.5\ \Omega & V_0 &= -48\ \text{kV} & C_2 &= 1.7\ \text{nF} \\ L_0 &= 208\ \text{nH} & L_1 &= 298\ \text{nH} & R_2 &= 28\ \Omega \end{aligned} \quad (1)$$

III. EXPERIMENTAL RESULTS

Figure 4 plots I_1 (MTG end) and I_2 (rail-gap end) as measured at opposite ends of one of the two trigger cables triggering the bank's two rail-gap switches during capacitor bank trigger/discharge tests to compare the cases of $R_2 = 28\ \Omega$ (damped) and $R_0 = 0\ \Omega$ (undamped). $R_0 =$

0 Ω is achieved by replacing the (30 cm long, 2.5 cm diameter carbon composite resistor with finger-stock end-caps) with an aluminum rod of similar dimensions to ensure similar inductance. All currents are measured with electronically RC integrated and numerically droop-corrected Rogowski coils. Figure 5 plots damped I_1 on a fore-shortened time scale to illustrate a much higher frequency oscillation than two which dominate on a longer time scale. The lumped circuit model, having two loops, is capable of representing the lowest two frequencies only.

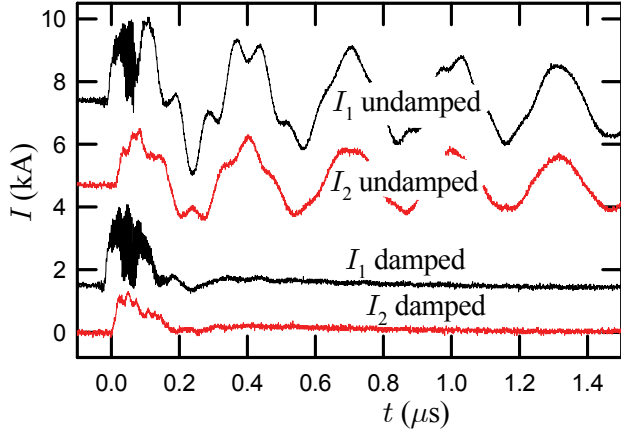


Figure 4. Trigger cable current at the MTG end I_1 and rail-gap end I_2 of the charged rail-gap trigger cable with damping resistor R_2 terminating the trigger cable after switch S_2 closure ($t = 0$) vs. the undamped case in which the resistor is replaced with an aluminum rod of similar dimensions. All currents start at 0 kA; vertical offsets are imposed only to avoid signal overlap.

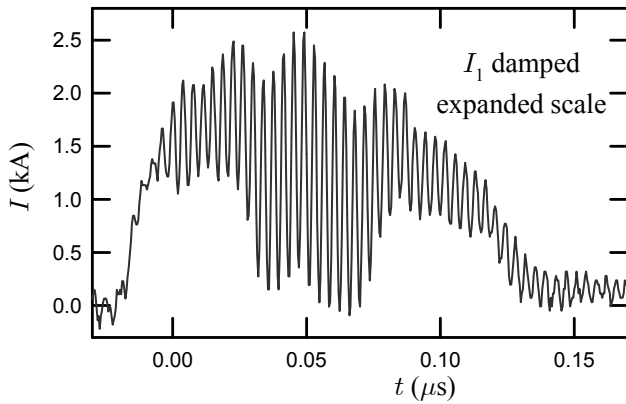


Figure 5. Detail of damped I_1 on a shorter time scale showing high frequency mode not representable by the lumped circuit model. The oscillation is not observed on I_2 and is unaffected by the damping resistor at that end.

IV. LUMPED CIRCUIT MODEL

From Kirchhoff's voltage law, the time derivatives of the voltages across each element of the two loops of the lumped circuit model in Fig. 3 after S_2 closure ($t > 0$) sum to zero. In matrix notation,

$$\begin{bmatrix} 1 + C_0 L_1 D^2 & -1 \\ -1 & 1 + C_0/C_2 + C_0 R_2 D + C_0 L_2 D^2 \end{bmatrix} \begin{bmatrix} I_1 \\ I_2 \end{bmatrix} = [0 \quad 0]^T \quad (2)$$

where D is the time derivative operator and, here and elsewhere, the r.h.s. term is transposed to save space (superscript T means to transpose back). This implies the determinant = 0 ,

$$(1 + C_2 R_2 D + (C_0 L_1 + C_2 L_1 + C_2 L_2) D^2 + C_0 C_2 L_1 R_2 D^3 + C_0 C_2 L_1 L_2 D^4) \begin{bmatrix} I_1 \\ I_2 \end{bmatrix}^T = 0 \quad (3)$$

which has the general solution,

$$\begin{bmatrix} I_1 \\ I_2 \end{bmatrix} = \sum_{k=1}^4 \begin{bmatrix} A_k \\ B_k \end{bmatrix} \exp(\Gamma_k t) \quad t > 0 \quad (4)$$

where the set $\{\Gamma_k\}$ are the two pairs of complex conjugate solutions to the quartic,

$$1 + C_2 R_2 \Gamma + (C_0 L_1 + C_2 L_1 + C_2 L_2) \Gamma^2 + C_0 C_2 R_2 L_1 \Gamma^3 + C_0 C_2 L_1 L_2 \Gamma^4 = 0 \quad (5)$$

We will generally solve this numerically. However, for cases where $R_2 = 0$ (undamped), the four solutions of the resultant *quadratic* in Γ^2 are,

$$\Gamma = \pm i \sqrt{\frac{b \pm \sqrt{b^2 - 4C_0 C_2 L_1 L_2}}{2C_0 C_2 L_1 L_2}} \quad (6)$$

$$b = C_0 L_1 + C_2 L_1 + C_2 L_2$$

After finding $\{\Gamma_k\}$ numerically or (if undamped) by Eqs. 6, initial conditions for I_1 , I_2 , DI_1 , and DI_2 are needed to determine specific solutions to the current waveforms. Plugging Eq. 4 into Eq. 2, the first row operation implies,

$$B_k = (C_0 L_1 \Gamma_k^2 + 1) A_k \quad (7)$$

Using this to eliminate $\{B_k\}$, the initial conditions for Eq. 4 may be written,

$$\begin{bmatrix} 1 & \dots & 1 \\ C_0 L_1 \Gamma_1^2 + 1 & \dots & C_0 L_1 \Gamma_4^2 + 1 \\ \Gamma_1 & \dots & \Gamma_4 \\ \Gamma_1 (C_0 L_1 \Gamma_1^2 + 1) & \dots & \Gamma_4 (C_0 L_1 \Gamma_4^2 + 1) \end{bmatrix} \begin{bmatrix} A_1 \\ A_2 \\ A_3 \\ A_4 \end{bmatrix} = [I_1 \quad I_2 \quad DI_1 \quad DI_2]_0^T \quad (8)$$

where subscript 0 means at $t = 0$ (the closing time of switch S_2). Inverting the matrix yields,

$$\begin{bmatrix} (\Gamma_1 - \Gamma_2) (\Gamma_1 - \Gamma_3) (\Gamma_1 - \Gamma_4) A_1 \\ (\Gamma_1 - \Gamma_2) (\Gamma_2 - \Gamma_3) (\Gamma_2 - \Gamma_4) A_2 \\ (\Gamma_1 - \Gamma_3) (\Gamma_2 - \Gamma_3) (\Gamma_3 - \Gamma_4) A_3 \\ (\Gamma_1 - \Gamma_4) (\Gamma_2 - \Gamma_4) (\Gamma_3 - \Gamma_4) A_4 \end{bmatrix} = \begin{bmatrix} \frac{\Gamma_2 + \Gamma_3 + \Gamma_4 - C_0 \Gamma_2 \Gamma_3 \Gamma_4 L_1}{C_0 L_1} & -\frac{\Gamma_2 + \Gamma_3 + \Gamma_4}{C_0 L_1} \\ -\frac{\Gamma_1 + \Gamma_3 + \Gamma_4 - C_0 \Gamma_1 \Gamma_3 \Gamma_4 L_1}{C_0 L_1} & \frac{\Gamma_1 + \Gamma_3 + \Gamma_4}{C_0 L_1} \\ \frac{\Gamma_1 + \Gamma_2 + \Gamma_4 - C_0 \Gamma_1 \Gamma_2 \Gamma_4 L_1}{C_0 L_1} & -\frac{\Gamma_1 + \Gamma_2 + \Gamma_4}{C_0 L_1} \\ -\frac{\Gamma_1 + \Gamma_2 + \Gamma_3 - C_0 \Gamma_1 \Gamma_2 \Gamma_3 L_1}{C_0 L_1} & \frac{\Gamma_1 + \Gamma_2 + \Gamma_3}{C_0 L_1} \end{bmatrix} \begin{bmatrix} I_1 \\ I_2 \\ DI_1 \\ DI_2 \end{bmatrix}_0 \quad (9)$$

where the 4×4 matrix above is spread out over three lines to fit the margins. Given initial conditions, this may be solved for $\{A_k\}$, with $\{B_k\}$ then found from Eq. 7. In this representation, real initial conditions will result in a real solution, despite the complex intermediate notation. This means that if the $\{\Gamma_k\}$ values are ordered such that the first two and last two coefficients are complex conjugate pairs, the $\{A_k\}$ and $\{B_k\}$ values will likewise be ordered as complex conjugate pairs. This detail facilitates the calculation of mode amplitudes.

Switches S_1 and S_2 are assumed to close at $t = -\tau_0$ and $t = 0$, respectively, based on the transit time $\tau_0 = 18.4$ ns of the trigger cable the model is intended to represent. Between these times, I_1 and V_1 are that of a single-loop LC series circuit discharge with,

$$\begin{aligned} I_1 &= -V_0 \sqrt{\frac{C_0}{L_1}} \sin\left(\frac{t + \tau_0}{\sqrt{L_1 C_0}}\right) \\ V_1 &= V_0 \cos\left(\frac{t + \tau_0}{\sqrt{L_1 C_0}}\right) \quad -\tau_0 < t \leq 0 \end{aligned} \quad (10)$$

The response of the second loop is initial purely inductive, so initial ($t = 0$) conditions for the subsequent two-loop behavior are,

$$\begin{bmatrix} I_1 \\ I_2 \\ DI_1 \\ DI_2 \end{bmatrix}_0 = \begin{bmatrix} -V_0 \sqrt{\frac{C_0}{L_1}} \sin\left(\frac{\tau_0}{\sqrt{L_1 C_0}}\right) \\ 0 \\ -\frac{V_0}{L_1} \cos\left(\frac{\tau_0}{\sqrt{L_1 C_0}}\right) \\ \frac{V_0}{L_2} \cos\left(\frac{\tau_0}{\sqrt{L_1 C_0}}\right) \end{bmatrix} \quad (11)$$

V. EXPERIMENTAL CORRELATION WITH MODEL

L_1 is inferred from documented MTG and cable properties. The MTG spark-gap inductance is inferred to be 40 nH when configured to drive 10 parallel 50 Ω cables

arranged symmetrically around its circumference. This is implied by the 8 ns e -fold (L/R) rise-time into 5 Ω quoted in the MTG manual[3]. The spark-gap drives two cables in our experiment, so it actually carries twice the lumped circuit model's I_1 . This can be represented in our single trigger circuit model by assuming $L_1 = L_0$ is twice the rated spark-gap inductance (80 nH). The inductance is theoretically slightly higher driving so few cables due to current feed asymmetry around the spark-gap, which is centered amongst the 10 possible cable lead locations. Approximating the 0.5 cm radius, 15 cm long cable lead into the MTG as a straight round conductor 4 cm from a ground plane representing a low inductance cylindrical feed to the spark-gap, the lead inductance adds about 10 nH, for a total of 90 nH. This is based on the inductance per unit length formula for two parallel round wires[4] (divided by two since one "wire" is only an image in the ground plane). Adding this to L_0 , based on the manufacturer's specification of 139 nH/m for a length of $D_0/2 = 1.5$ m, gives $L_1 = 298$ nH.

L_2 , meanwhile, is more easily inferred empirically from the presented data due to the convoluted nature of the rail-gap trigger feed (Fig. 2). Although a two loop circuit can only describe two real frequencies, three such frequencies with periods of 287×10^{-9} s, 84.5×10^{-9} s, and 3.85×10^{-9} s characterize the waveforms recorded for I_1 and I_2 . The second period is measured from the numerically time differentiated undamped I_1 waveform. The amplitude of the second frequency is greater than the first in this representation, permitting the time elapsed for 11 oscillations to be measured accurately. The (3 m polyethylene insulated) cable has a transit time of 18.4 ns, so the highest frequency corresponds a cable mode not representable by the lumped circuit model. We hypothesize, though, that the first (lowest frequency) mode, which dominates the signal, may be represented by our two-loop model. The angular frequency magnitude for this is $\omega = 2.19 \times 10^7$ s $^{-1}$. Solving Eq. 5 with $R_2 = 0$ for L_2 , we get,

$$L_2 = \frac{1 - \omega^2 (C_0 L_1 + C_2 L_1)}{\omega^2 C_2 - \omega^4 C_0 C_2 L_1} \quad \omega = -i\Gamma \quad (12)$$

This gives $L_2 = 889$ nH. This and other circuit parameters are summarized in Eqs. 1

For the (undamped) case of $R_2 = 0$ Ω , we have from Eqs. 6 $\{\Gamma_k\}$ values of $\pm 2.190 \times 10^7 i$ s $^{-1}$ and $\pm 7.51 \times 10^7 i$ s $^{-1}$, corresponding to periods of 287 ns and 83.6 ns, respectively. The longer period is, by assumption, exactly that measured and used for our assignment of L_2 in Eqs. 12. However, we have obtained a good match for the 84.5 ns period mode observed. For the (damped) case of $R_2 = 28.0$ Ω , we have from Eq. 5 numerically determined $\{\Gamma_k\}$ values of $(-1.15 \pm 1.92i) \times 10^7$ s $^{-1}$ and $(-0.43 \pm 7.36i) \times 10^7$ s $^{-1}$, corresponding to similar periods as before, but with strong damping (comparable imaginary and real components) for the lowest frequency,

and weaker damping (with a $23 \mu\text{s}$ decay time) for the higher. These frequency and damping results are in substantive agreement with the measurements (Fig. 4).

Using the parameter values in Eqs. 1 and initial conditions from Eq. 11 in Eq. 9 to determine $\{A_i\}$, and then Eq. 7 to determine $\{B_i\}$, I_1 and I_2 are found from Eq. 4 for the damped and undamped $\{\Gamma_k\}$ cases above. The mode amplitudes for the high (amplitude coefficients 1 and 2, by convention) and low (coefficients 3 and 4) frequencies for the undamped case are,

$$\begin{aligned} 2\sqrt{A_1A_2} &= 1.809 \text{ kA} & 2\sqrt{A_3A_4} &= 0.706 \text{ kA} \\ 2\sqrt{B_1B_2} &= 0.687 \text{ kA} & 2\sqrt{B_3B_4} &= 0.624 \text{ kA} \end{aligned} \quad (13)$$

The amplitudes for the damped case are similar. The most significant discrepancy with the experimental data is that, while the low frequency dominates the experimental measurements, the higher frequency dominates in the model. The significant degree of isolation of the higher frequency mode to the MTG end (i.e. the amplitude is much higher there) is, nonetheless, well represented. To illustrate these characteristics, Fig. 6 plots the detailed time dependence of the undamped vs. damped cases for I_1 and I_2 , for comparison with Fig. 4. As shown in the $t < 0$ portion of the I_1 trace, the higher of the two modeled modes is similar to the single loop frequency of I_1 assumed prior to S_2 closure (Eqs. 10). It having a lower amplitude in I_2 , then, is due to low coupling efficiency.

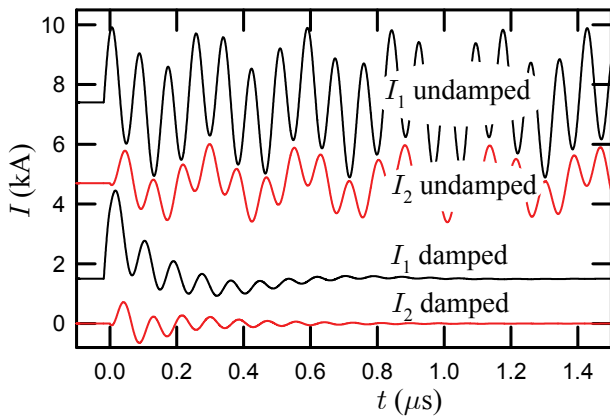


Figure 6. I_2 for the undamped and damped (terminated) cases of the lumped circuit model for comparison with the experimental results of Fig. 4.

VI. CONCLUSIONS

The lumped circuit model is adequate to identify the two highest amplitude long-lived frequencies of the charged cable trigger, in addition to their decay times and the degree of isolation of the higher frequency mode to the MTG end. The relative amplitudes of the two modes, however, are not well modeled due to an inability to represent the initial fast transmission line behavior via initial

conditions of the lumped circuit model. Efforts to contrive initial conditions so as to reproduce the experimental current traces of Fig. 4 were highly successful (except for the very high frequency oscillation shown in Fig. 5). However, this adds little information beyond the fact that the frequencies, damping rates, and isolation of the higher frequency to the MTG side for the model agree with the experiment, as already noted. For a predictive model that includes accurate amplitudes and represents the highest frequency observed (Fig 5), a continuous transmission line model is needed.

Resistive termination of the output of the trigger cable of a rail-gap switching circuit proves useful for damping resonant modes within the cable circuit. This reduces RF interference with electronic system diagnostics. As a result of this effort and general improvements in the RF isolation of the electric and magnetic field diagnostics that motivated them, RF pickup has been reduced to negligible levels compared to other sources of noise. These results are omitted here because the diagnostics themselves were improved concurrently, so no controlled comparison is available. The diagnostics work quite well without trigger damping now, for example. In hindsight, surrounding the trigger circuit elements at the rail gap end by multiple return paths, as pictured in Fig. 2, reduces radiation from the trigger cable break-out. This may indeed be at least as effective at reducing interference elsewhere as the damping resistor itself.

VII. REFERENCES

- [1] C. Grabowski, J. Degnan, T. Cavazos, D. Gale, C. Gilman, W. Sommars, T. Intrator, J. Taccetti, B. Waganaar, R. Siemon, and G. Wurden, "Development of a high-current low-inductance crowbar switch for FRX-L", IEEE Trans. Plasma Sci., vol. 30, no. 5, pp. 1905–1915, 2002.
- [2] Instructions for Using the Model 40200 Rail-Gap Switch, 1986, Maxwell Laboratories Manual TGM-151, 8888 Balboa Ave. San Diego, CA 92123.
- [3] Instructions for Using the Model 40151-B 100 kV Multiple Trigger Generator, Maxwell Laboratories Manual MLR-2358A, 8888 Balboa Ave. San Diego, CA 92123.
- [4] J. D. Huba, NRL Plasma Formulary, Revised, 1998 (Naval Research Laboratory NRL/PU/6790-94-265, Washington, DC).